Journal of Structural Geology, Vol. 14, No. 5, pp. 579 to 589, 1992
Printed in Great Britain

0191-8141/92 $05.00+0.00

A fluid inclusion study of fluid pressure and salinity variations in the footwall of the Rector Branch thrust, North Carolina, U.S.A.

KIERAN O'HARA and AMY HAAK*

Department of Geological Sciences, University of Kentucky, Lexington, KY 40506, U.S.A.

(*Received* 21 *May* 1991; *accepted in revised form* 11 *November* 1991)

Abstract—Last melting and homogenization temperatures of fluid inclusions from plastically deformed bedding-parallel quartz veins in the footwall of the Rector Branch thrust, North Carolina, were studied as a function of distance from the thrust. Fluid inclusions and microstructures in mylonitic rocks within the thrust zone were also examined. Fluid inclusions in quartz veins which display evidence for intracrystalline plasticity (e.g. subgrain polygonization) occur along subgrain boundaries and have higher homogenization temperatures (T_h) and a wider range (120–320°C) compared to less deformed samples. Maximum T_h values, which approach the temperature of deformation (300 ± 20°C), apparently reflect leakage of inclusions along subgrain boundaries. Minimum T_h values (120–160°C), on the other hand, record near lithostatic conditions (2.6 kb) at 300°C.

Maximum last melting temperatures (T_m) increase from −20 to −4°C with decreasing distance to the thrust, corresponding to a decrease in salinity of the fluid from 23 to 3 wt% (NaCl equivalent). The decrease in salinity towards the fault is interpreted as due to infiltration of the fault at depth (to approximately 10 km) by surface derived waters during periods of fault zone dilatancy. Inclusions along healed microcracks in quartz from the fault zone display higher salinity (17–26 wt% NaCl equiv.) and are interpreted to reflect enhanced fluid–rock interaction in the fault zone due to hydration reactions. The fluid pressure and salinity variations are consistent with a combined dilatancy–hydraulic fracturing model for the Rector Branch thrust. Previously documented bulk rock volume losses for this fault zone are inferred to have been produced by the fluxing of the fault zone with undersaturated surface derived fluids.

INTRODUCTION

SEVERAL studies have suggested that ductile shear zones in the continental crust have been infiltrated syntectonically by large volumes of fluid (e.g. Sinha *et al.* 1986, Reynolds & Lister 1987, O'Hara 1988, Kerrich 1989, Losh 1989). In many cases fluid infiltration was accompanied by large bulk-rock volume loss reflected by losses of alkalies and silica (e.g. O'Hara & Blackburn 1989, Glazner & Bartley 1991, Selverstone *et al.* 1991). Because the solubility of silica in aqueous metamorphic fluids is low and is not strongly dependent on salinity (Fournier *et al.* 1982) the silica losses imply large fluid/rock volume ratios (10^2–10^3) and large fluid fluxes (10^8–10^9 cm^3 cm^{-2}; Ferry & Dipple 1991).

Considerable uncertainty concerning the source (e.g. connate, meteoric, metamorphic, etc.) or the circulation pattern of these fluids (e.g. single pass, multiple pass) exists (e.g. Kerrich 1989). Convective circulation of metamorphic fluids can explain high fluid/rock ratios (Etheridge *et al.* 1983), but whether fluids can convectively circulate against the lithostatic gradient in metamorphic terranes has been questioned (e.g. Valley 1986, Wood & Walther 1986). On the other hand, tectonic pumping of high-level fluids along active faults and shear zones has been proposed (Scholz *et al.* 1973, Sibson *et al.* 1975, Costain *et al.* 1987, McCaig 1988). Because mylonites which formed under brittle–plastic conditions commonly show evidence for hydraulic fracturing as well as dilatant behavior (e.g. Simpson 1986, Stel 1986) and experimental studies show that dilatancy can occur under high temperature conditions (Fischer & Paterson 1989) the downward migration of surface derived fluids under near hydrostatic conditions into brittle–plastic shear zones might be expected. Additionally, such fluids would migrate in the direction of increasing temperature and pressure and their solute-carrying capacity would be enhanced, making them effective agents of dissolution and volume loss.

Fluid inclusion studies are playing an increasingly important role in understanding fluid–rock interaction in the vicinity of faults and shear zones (Lespinasse & Cathelineau 1990, Parry & Bruhn 1990). In addition to structural considerations (e.g. Sibson *et al.* 1975) these studies provide evidence for cyclic fluctuations in fluid pressure between lithostatic and hydrostatic conditions. This study reports on fluid inclusion characteristics from bedding-parallel quartz veins in the footwall of the Rector Branch thrust, North Carolina.

TECTONIC SETTING

The Hot Springs window is situated in the western Blue Ridge province of the southern Appalachians (Fig. 1), where Grenville-aged (approximately 1 Ga) crystalline gneisses were thrust during Paleozoic time onto late Precambrian metasedimentary rocks of the Snowbird Group. The eastern and southern margins of the window are bounded by the Rector Branch thrust (Oriel 1950, fig. 1). Previous studies indicate that greenschist grade mylonites, developed in the granitic rocks of the hangingwall of the Rector Branch thrust, experienced large volume losses (O'Hara 1988, 1990).

*Present address: 1375 Magazine St., New Orleans, LA 70130, U.S.A.

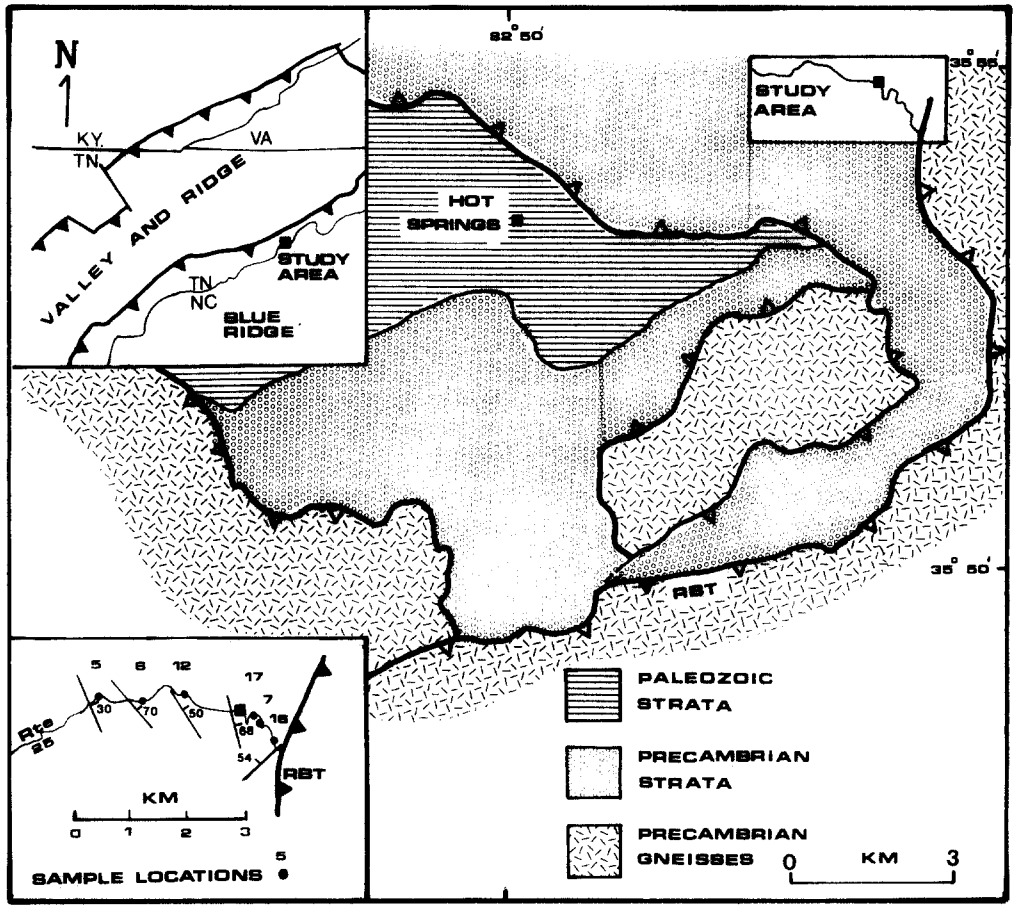

Fig. 1. Generalized geologic map of the Hot Springs window, North Carolina (after Oriel 1950). The location of a sampling traverse in the footwall of the Rector Branch thrust (RBT) is shown (lower left inset). Paleozoic strata comprise Cambrian carbonates and clastic metasedimentary rocks. Precambrian strata comprise late Precambrian metasedimentary clastic rocks. Teeth are on the upper plate of thrust faults.

METHODS AND RESULTS

Fluid inclusions in six samples of quartz veins within the Snowbird Formation were examined along a 4 km E–W traverse in the hangingwall of the thrust (inset, Fig. 1). Fluid inclusions in samples from deformed rocks within the fault zone were also examined. These inclusions occur along healed microfractures as opposed to within veins. Microstructural observations on all samples were made on regular petrographic thin sections. Fluid inclusion measurements were made on doubly polished thick (100 μm) sections using a USGS heating–cooling stage, modified by Fluid Inc. The stage was calibrated at the boiling point of pure liquid nitrogen (−195.8°C), in an ice bath of distilled water (0°C), and at the critical point of water (374.1°C). Fluid inclusions are all two phase liquid–vapor inclusions (1–10 μm in size) with most in the range of 3–5 μm. For inclusions of this size a cycling technique (Roedder 1984, p. 197) was usually employed. Homogenization temperatures were determined within a range not exceeding 5°C using this technique. Homogenization was in all cases to the liquid phase. Repeated measurements on single inclusions indicate an accuracy of ±0.5°C during freezing runs. The equation of Potter *et al.* (1978) was used to convert last melting of ice temperatures to salinity; all salinities are expressed as weight% NaCl equivalent.

Fault zone rocks

The rocks of the Rector Branch thrust are strongly foliated, retrogressed granitic gneisses. Point-counting reveals that the major modal changes between the protolith gneisses and the fault zone rocks are a decrease in quartz and alkali feldspar and an increase in white mica, chlorite and epidote (Haak 1990). Similar modal changes were also observed further to the south along the same fault (O'Hara 1990). Biotite is usually replaced by chlorite, which together with secondary epidote, gives the fault zone rocks a green coloration in outcrop.

Quartz veins at a high angle to the foliation are common. Quartz in the fault zone is observed to undergo grain-size reduction by fracturing (Fig. 2a) but also shows evidence for intracrystalline plasticity. Quartz grains display sweeping undulatory extinction and locally new finer strain-free grains are observed within larger fractured grains and also along grain margins. Some grains show elongation parallel to the foliation, but the length–width ratios are generally <2. Fractures between quartz fragments are filled with chlorite and/or muscovite (Fig. 2a). The irregular shape and disconnected occurrence of quartz throughout the rock matrix (Fig. 2a) suggest that quartz initially obtained its shape by brittle processes. At advanced stages of deformation, however, quartz shows evidence for

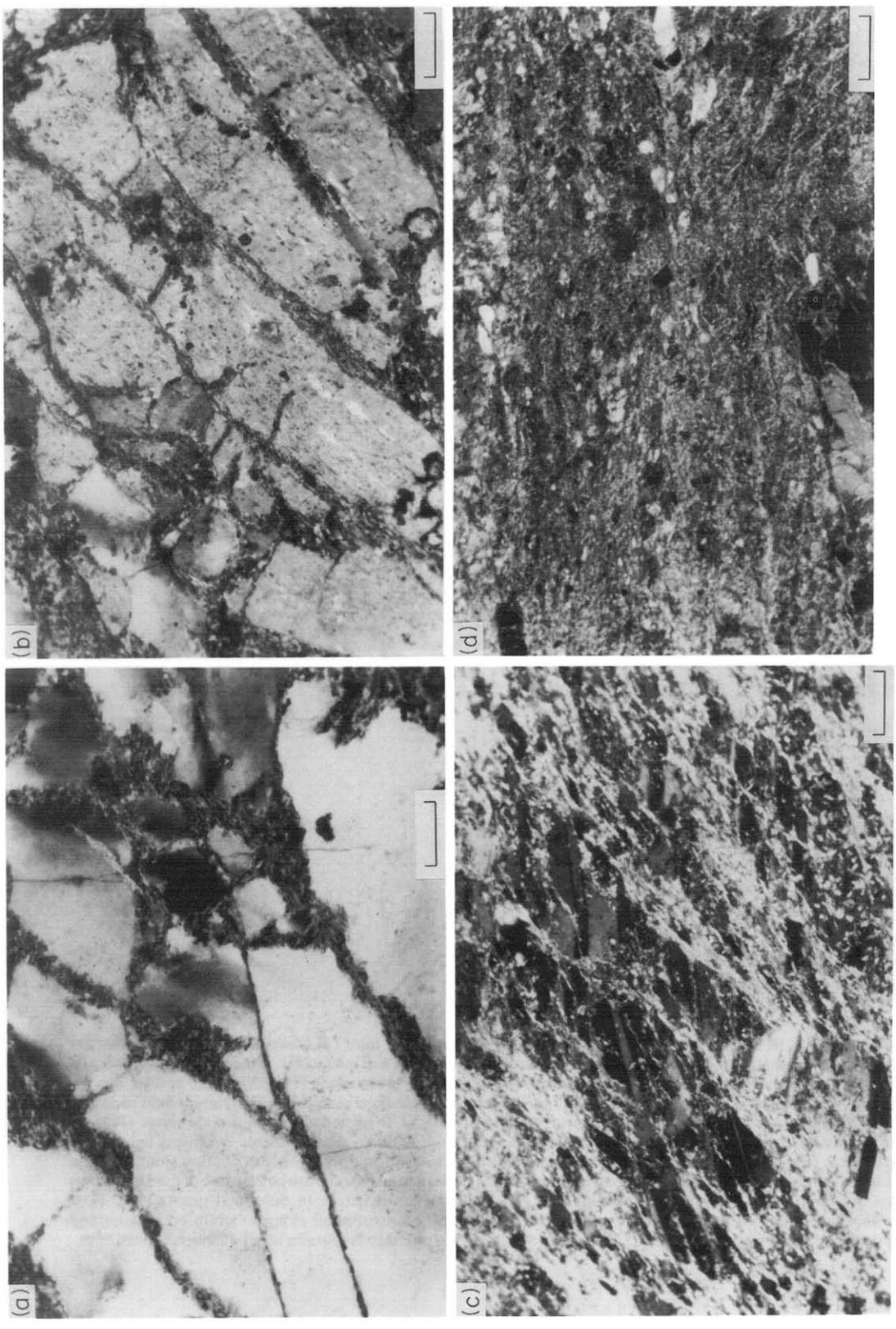

Fig. 2. Photomicrographs of lower greenschist facies mylonitic gneisses from the Rector Branch fault zone from the northeastern margin of the window (Fig. 1). (b)–(d) show evidence for hydration reactions involving feldspar hydrolysis. All scale bars 0.2 mm, except (d) which is 1 mm. (a) Quartz showing grain-size reduction by fracture. Individual fragments, however, display sutured margins and undulatory extinction, indicating overprinting by crystal-plastic deformation. Fractures are filled with chlorite. Polarized light. (b) Alkali feldspar displaying shear fractures at a high angle to the foliation which is E–W. Fractures are lined with chlorite and muscovite. Polarized light. (c) Plagioclase feldspar showing extensive chemical breakdown to white mica along fractures. Feldspar grains have become flattened and elongated parallel to the foliation by cataclastic flow. (d) East–west microshear in mylonitic gneiss. Grain-size reduction of feldspar was by brittle processes. Quartz shows evidence of deformation by both brittle deformation and syntectonic recrystallization.

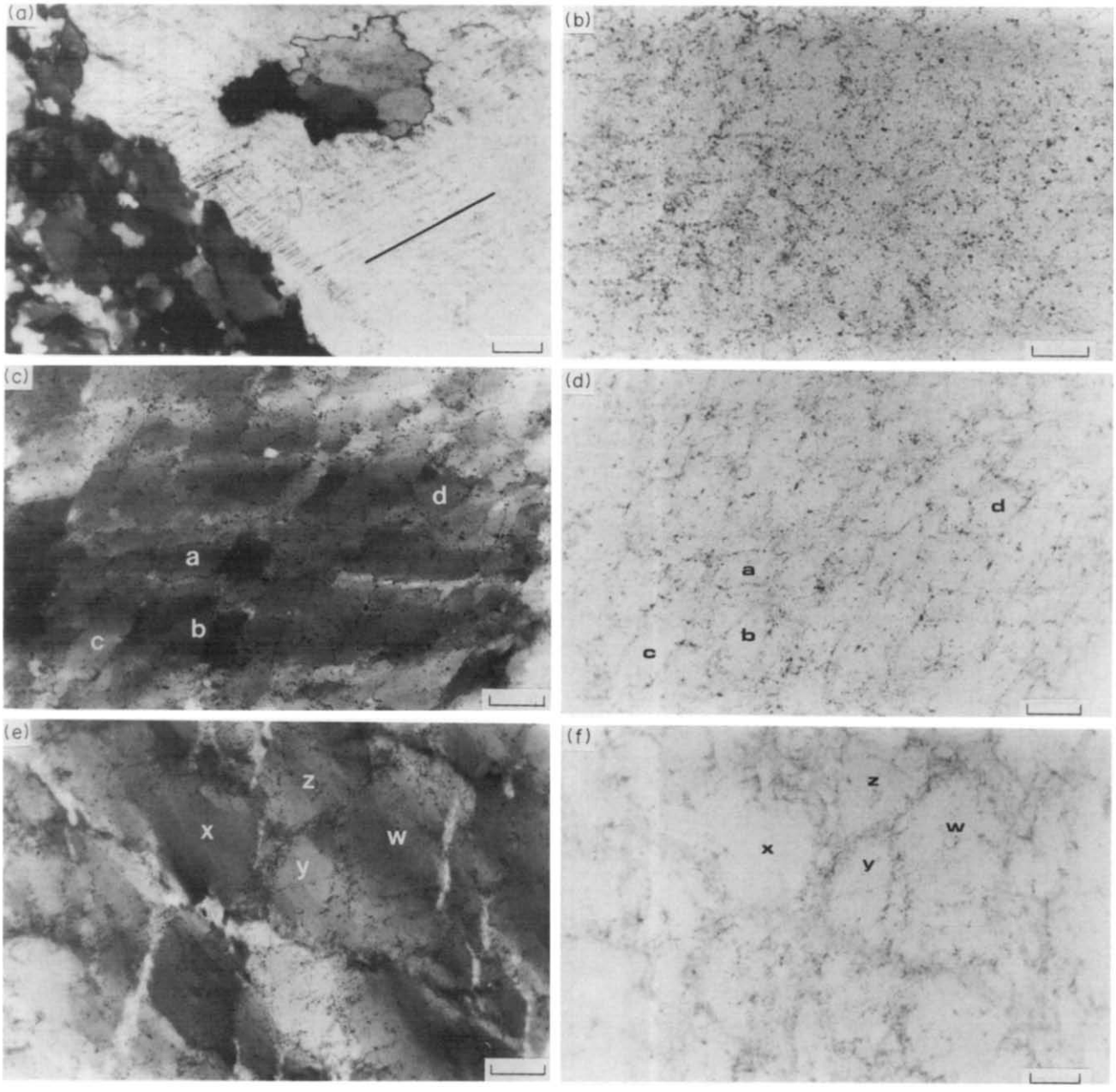

Fig. 3. Photomicrographs of microstructures in vein quartz. All scale bars 0.2 mm. (a) Quartz vein (location 5, Fig. 1) displaying crack–seal texture, overprinted by newly recrystallized grains (center and lower left). Fluid inclusion homogenization temperatures in non-recrystallized areas display a narrower range and a lower mode (e.g. locations 5 and 16, Fig. 4). Polarized light. (b) Polygonal distribution of fluid inclusions in plastically deformed quartz vein. Maximum fluid inclusion homogenization temperatures for samples displaying this texture are 300°C or higher and show a wide range (Fig. 4). (c) Quartz microstructure in plastically deformed quartz vein showing subgrain development. Polarized light. Four subgrains are labeled. (d) Same as (c) in plane-polarized light. Fluid inclusions show a polygonal distribution along subgrain boundaries. Labeled areas (a, b, c and d) correspond to subgrains in (c). Subgrain interiors are largely free of fluid inclusions and inclusions are distributed along subgrain boundaries. (e) Quartz microstructure in deformed quartz vein. Four subgrains are labeled. Polarized light. (f) Same as (e). Fluid inclusions are distributed along subgrain boundaries and subgrain interiors are largely free of inclusions. Clear areas (w, x, y, z) correspond to subgrains in (e). Plane-polarized light.

grain-size reduction by syntectonic recrystallization (Fig. 2d).

In contrast to quartz, feldspar undergoes grain-size reduction entirely by brittle processes. Fractures in feldspar in weakly deformed samples are oriented at a high angle to the foliation and are filled with phyllosilicates (Fig. 2b). Bookshelf-type shears are commonly developed, which in more intensely deformed samples are rotated into parallelism with the foliation. Fragmented feldspar grains become elongated parallel to foliation—the change in shape fabric being accommodated by shear between fragments. These microshears are lined with phyllosilicates (chlorite and mica) and also epidote (Fig. 2c). Both the mechanical and the chemical breakdown of the feldspars, either to masses of epidote and chlorite or white mica, is locally extensive along microshears within the protolith (Fig. 2d). The above microstructural observations and modal changes suggest the following reactions were important in the fault zone:

$$3/2\text{K-spar} + H^+ = 0.5\text{Muscovite} + 3SiO_2 + K^+ \quad (1)$$

$$\text{K-spar} + \text{Oligoclase} + 0.5H_2O + 3.5H^+ = \text{Epidote} + \text{Muscovite} + 11SiO_2 + 4Na^+. \quad (2)$$

Two-phase liquid–vapor fluid inclusions are present along healed microfractures in quartz and they homogenize (to liquid) between 125 and 205°C with a mode at 150°C ($n = 25$; Haak 1990). Last melting temperatures (−13 to −24.5°C) indicate fluid salinities of 17–26 wt% ($n = 16$). First melting temperatures (−25.5 to −32.5°C; $n = 5$) suggest solutes in addition to NaCl and K_2O were present (e.g. $CaCl_2$; Crawford *et al.* 1979).

The absence of extensive quartz plasticity is consistent with the chlorite grade of greenschist facies metamorphism. This is in contrast to biotite grade present along the southern margin of the window where mylonitic quartz ribbons are common (O'Hara 1988). In light of the absence of extensive intracrystalline plasticity in quartz and the brittle behavior of feldspar these rocks might be termed foliated cataclasites rather than mylonites. Regardless of terminology, however, the observed microtextures suggest dilatant behavior (e.g. Fig. 2b) and indicate the rocks deformed in the semibrittle mode. Macroscopically these rocks behaved ductilely but deformation in the fault zone is heterogeneous on the outcrop and hand specimen scales.

Homogenization temperatures in quartz veins

The quartz veins sampled occur within the Snowbird Group in the footwall of the thrust and all are bedding-parallel veins of variable thickness (1–20 cm) and extent. The abundance of veins in outcrop increases towards the thrust. Chlorite is common in the veins and calcite rare. Quartz in all the veins examined shows evidence of intracrystalline strain, including sweeping undulatory extinction, deformation bands, subgrain development and less commonly, strain-free dynamically recrystallized grains. Some veins locally show syntectonic recrystallization but these areas do not contain usable fluid inclusions, suggesting recrystallization has locally destroyed the inclusions. The quartz–chlorite assemblage in the veins and the similarity of the quartz vein microstructures to those in the fault zone, together with an increase in veining toward the fault, suggest the veins are related to faulting. Histograms of homogenization temperatures (T_h) and last melting temperatures (T_m) are shown in Figs. 4 and 5, respectively, for the samples examined (inset, Fig. 1).

In the least deformed sample (inset Fig. 1, location 5) inclusions occur along numerous closely spaced, subparallel, healed microfractures, producing a texture similar to crack–seal structure (Ramsay 1980). Locally, this texture is overprinted by newly recrystallized finer grains which annihilate the fluid inclusions (Fig. 3a). The homogenization temperatures of inclusions for this sample show a unimodal distribution and a relatively narrow range (Fig. 4, location 5).

In more deformed samples, the fluid inclusions display a polygonal distribution (Fig. 3b). In polarized light, quartz in these samples displays extensive subgrain development and it is clear that the polygonal distribution of fluid inclusions is due to subgrain development in quartz (compare Fig. 3c with 3d, and Fig. 3e with 3f). The subgrains have a range in crystallographic misorientation with respect to neighboring grains, most being less than 10°. Those with substantially higher misorientation represent newly recrystallized grains. The development of a polygonal microstructure due to subgrain formation is referred to as creep polygonization and reflects recovery by dislocation creep processes (Poirier 1985, p. 170). In these polygonized samples fluid inclusions have been swept from the interior of the subgrains and are now redistributed along subgrain boundaries (Figs. 3b,d & f). Most of these inclusions are too small to obtain data from. Commonly, however, larger (3–5 μm) fluid inclusions are present within the newly formed subgrains and also along the subgrain boundaries. These inclusions commonly have large vapor bubbles and a wide range (e.g. Fig. 4, location 12) or high (e.g. Fig. 4, location 7) homogenization temperatures suggesting a relationship between T_h and deformation.

In order to examine the relationship between deformation and T_h, the maximum, mode and minimum homogenization temperatures from Fig. 4 are plotted as a function of distance from the surface trace of Rector Branch thrust in Fig. 6(a). If sample 16, which is closest to the fault, is omitted, the modal homogenization temperature shows a tendency to increase with decreasing distance to the fault. If, on the other hand, sample 7 is omitted, a peak in T_h is observed 2 km from the fault. Contrary to expectation, petrographic examination of sample 16 does not indicate an extensively polygonized microstructure. Also contrary to expectation, sample 12 which is 2 km from the fault, does display a highly polygonized microstructure. These observations suggest that proximity to the fault is not a good indication of intensity of deformation.

Petrographic observations do indicate, however, that weakly polygonized samples (e.g. samples 5 and 16)

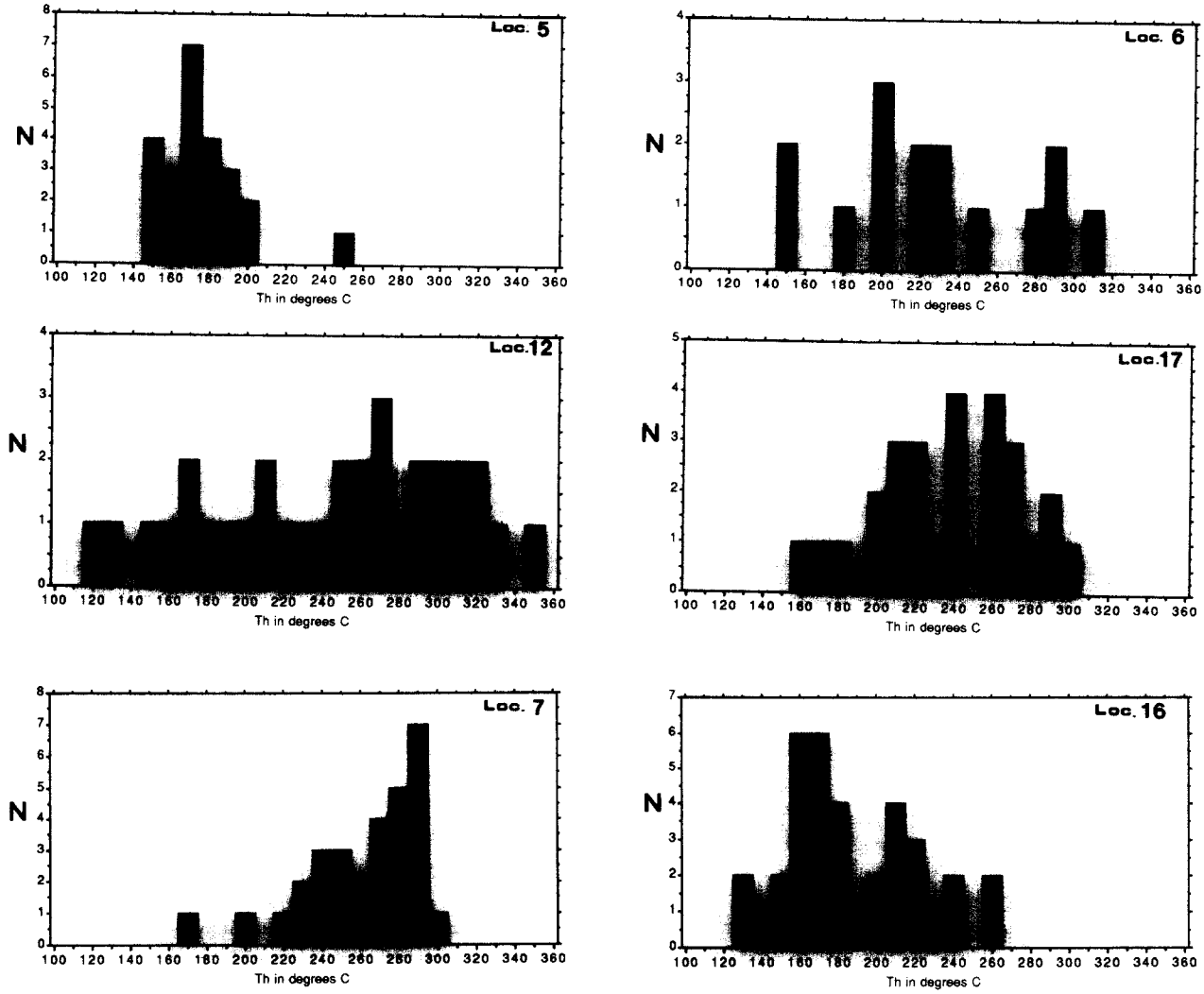

Fig. 4. Histograms of fluid inclusion homogenization temperatures for sample locations shown in Fig. 1. Locations 5 and 16, which display a narrow range of T_h and/or lower T_h values, display only local recrystallization and minor subgrain development (e.g. Fig. 3a). Other samples which display extensive subgrain development (e.g. Figs. 3c & d) show a wider range and higher homogenization temperatures. The higher T_h values in the more deformed samples are attributed to a decrease in fluid density during or after intracrystalline plastic deformation.

display a narrower range and lower T_h values (Fig. 4) whereas highly polygonized samples (e.g. Fig. 3) display a larger range and higher T_h values (e.g. samples 12 and 7, Fig. 4). These relationships suggest that crystal-plastic deformation may have resulted in producing higher T_h values through either inclusion leakage or other fluid density changes. Kerrich (1976) observed a similar relationship between T_h and deformation in partially recrystallized quartz. The distribution and morphology of fluid inclusions in quartz veins which have undergone creep polygonization have many similarities to those along grain boundaries in quartz tectonites described by White & White (1981). The 'sweeping clean' of newly recrystallized grains of fluid inclusions has been described previously in naturally deformed quartz (Kerrich 1976, Wilkins & Barkas 1978) and also in experimental studies (Drury & Urai 1990).

Fluid salinity in quartz veins

In contrast to homogenization temperatures, the salinity of fluid inclusions, as reflected in last melting of ice temperatures, is not sensitive to volume or density changes (Sterner & Bodnar 1989) and, provided the inclusions have remained closed systems, their salinities are accurate reflections of the fluid salinity at the time of trapping. First melting temperatures of inclusions in vein quartz, which provide information on the composition of the fluids, range from −23 to −37°C indicating solutes (e.g. $CaCl_2$ or $MgCl_2$, Crawford *et al.* 1979) in addition to NaCl are present in the fluids.

Histograms of last ice melting temperatures are presented in Fig. 5. Figure 6(b) shows the minimum, mode and maximum of these data plotted as a function of distance from the fault. The maximum last melting temperatures show an increase with decreasing distance from the thrust. This corresponds to a decrease in salinity from a maximum value of 23 wt% away from the fault to minimum value of 3.3 wt% close to the fault (Fig. 6b). This decrease in salinity corresponds to an eight-fold dilution. It is interesting to note that in several samples only the minimum salinity decreases and the maximum salinity is preserved.

The decrease in salinity as a function of distance from

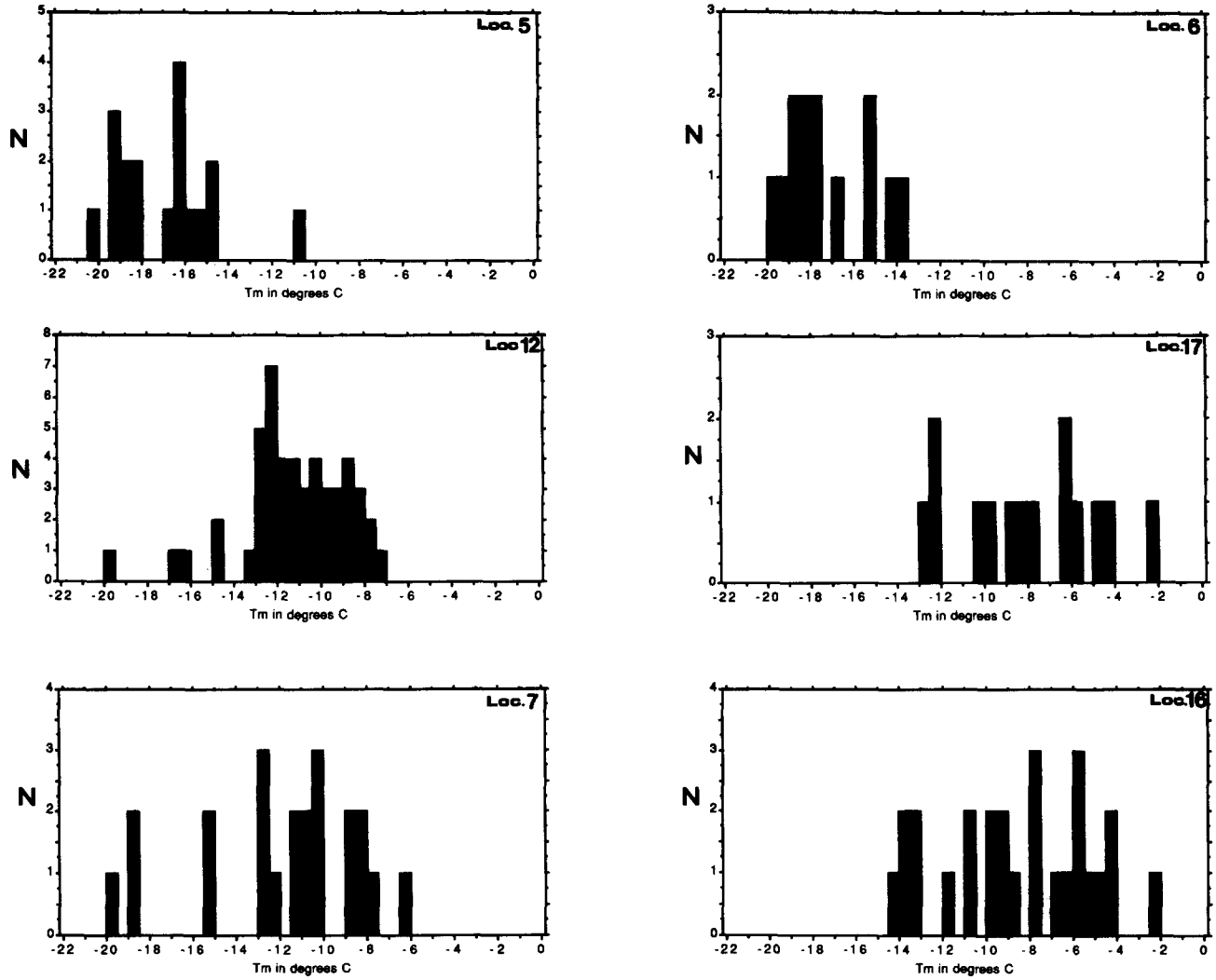

Fig. 5. Histograms of last melting temperatures (T_m) for sample locations shown in Fig. 1. Maximum T_m values show a decrease with decreasing distance from the fault corresponding to a decrease in fluid salinity towards the fault (Fig. 6b).

the fault requires mixing with a low salinity fluid source. Several sources suggest themselves—meteoric waters, metamorphic dehydration fluids and connate or formation waters. For example, metamorphic dehydration reactions near the fault zone could supply a low salinity fluid if fluid flow was focused along the fault zone. However, most of the reactions in the fault zone involve hydration rather than dehydration (e.g. reactions 1 and 2 above). In addition, an obvious source of dehydrating rocks is not apparent—the Snowbird Group was apparently deformed and metamorphosed prior to thrusting (Oriel 1950). Similarly, a source of connate or formation waters from unmetamorphosed sedimentary rocks is not readily available. Moreover, formation or connate fluids tend to increase in salinity with depth and can be expected to be moderately to highly saline (Hanor 1976, Frape & Fritz 1986). These considerations suggest that surface-derived (e.g. meteoric) fluids may have infiltrated the fault zone to depth. This could occur following hydraulic fracturing when fluid pressure conditions were temporally reduced or during pre-rupture dilatancy when permeability is high (see Discussion).

Fluids trapped along healed microfractures within the fault zone have lower homogenization temperatures and higher salinities compared to fluids trapped in vein quartz (Fig. 7). The higher salinity of the microcrack inclusions is not inconsistent with the suggestion above that a low salinity fluid infiltrated the fault zone. The higher salinity may be explained by grain-scale fluid–rock interaction in the fault zone, in which removal of H_2O and release of solutes such as K^+ and Na^+ (reactions 1 and 2 above) to the fluid locally increased the salinity of the fluid (Crawford *et al.* 1979). The lower T_h of the microcrack inclusions may reflect lower temperature (and possibly later) inclusions compared to the quartz veins or they may reflect locally higher fluid pressures (and densities). Regardless of which interpretation is correct, the evolution or origin of fluids trapped along healed microfractures in the fault zone appears to have been distinct from that of fluids present in veins. The relationship between salinity and T_h in Fig. 7 suggests that mixing of these two distinct fluids may have occurred.

The occurrence of the fluid inclusions along subgrain boundaries (Figs. 3b,d & f) rather than along healed trails in quartz veins suggests the low salinity fluid inclusions are not the result of late stage influx of surface fluids along brittle fractures. In addition, such low

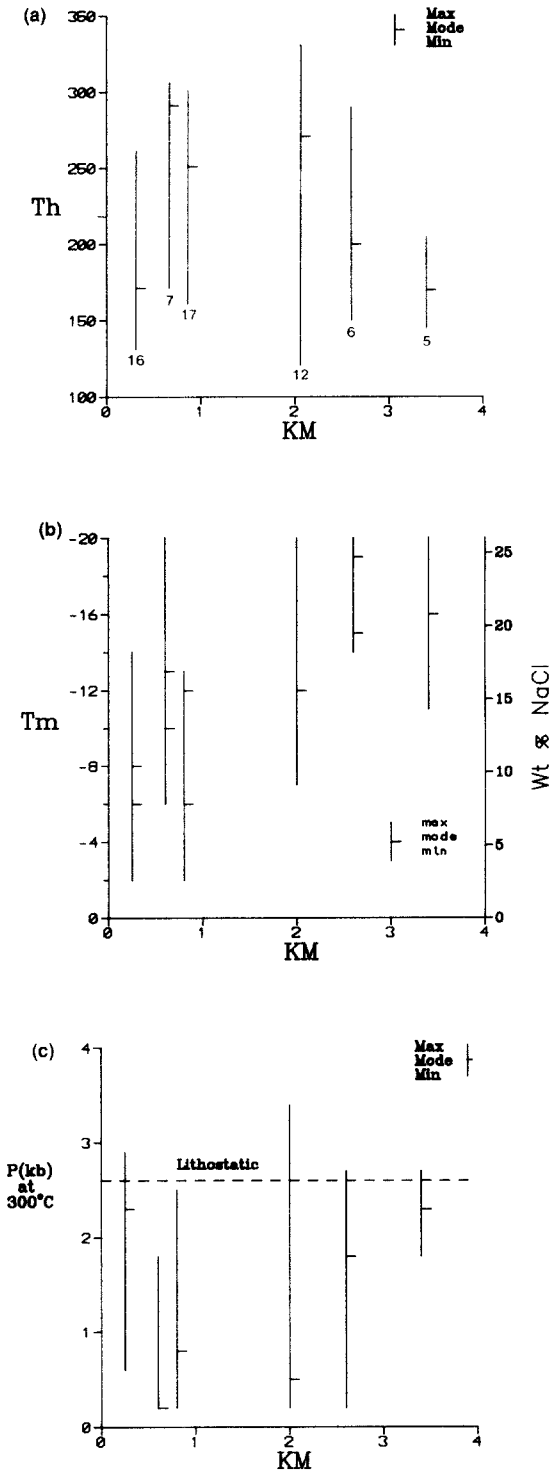

Fig. 6. (a) Range in homogenization temperatures plotted against distance from the Rector Branch thrust. The sample number for each location is indicated. See text for discussion. (b) Plot of last melting temperature and percentage salinity (NaCl equivalent) vs distance from the fault. The minimum salinity tends to decrease towards the fault. The decrease in salinity is interpreted as due to infiltration of low salinity surface-derived fluid into the fault zone at depth. (c) Plot of calculated fluid pressures at 300°C as a function of distance from the fault, based on data in Table 1. A lithostatic pressure of 2.6 kbar (260 MPa) is indicated assuming a geotherm of 30°C km^{-1} and a rock density of 2600 kg m^{-3}. The maximum pressures indicated are close to lithostatic, consistent with formation of the quartz veins by hydraulic fracturing followed by pressure release and quartz precipitation. The minimum fluid pressures indicated in deformed samples are interpreted to reflect decrease in fluid density due to crystal-plastic deformation rather than sub-hydrostatic fluid pressure.

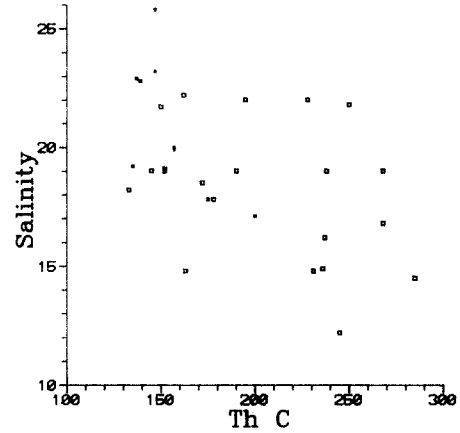

Fig. 7. Plot of homogenization temperature vs salinity for those inclusions on which both measurements were made. Closed squares represent inclusions along healed microfractures from Rector Branch fault zone rocks. Open squares represent inclusions from quartz veins. Fault zone inclusions have higher salinities and lower T_h values compared to vein quartz.

temperature, low salinity fluids would be expected to display low rather than high T_h values, but this is not observed (Fig. 7). The dilute fluids must have gained access to the fault during intracrystalline plasticity of quartz at depth.

INTERPRETATION OF HOMOGENIZATION TEMPERATURES

The homogenization temperature of fluid inclusions present along subgrain boundaries provides some insight into the density and pressure conditions of entrapment. The higher T_h of inclusions in deformed samples indicates that these inclusions re-equilibrated to lower densities. The re-equilibration of fluid inclusions to lower densities may occur by inelastic volume change, decrepitation, or diffusion and leakage, and these processes have been experimentally investigated by several workers (e.g. Pêcher 1981, Gratier & Jenatton 1984, Prezbindowski & Laresse 1987, Sterner & Bodnar 1989, Bakker & Jansen 1990). Prezbindowski & Laresse (1987) showed that heating of calcite inclusions resulted in stretching of the inclusion, and consequently lowering of the fluid density. This resulted in 'isochore jumping' whereby the stretched inclusion followed a lower density isochore in P–T space. The result was an increase in the homogenization temperature such that it approached the maximum temperature conditions during re-equilibration. More recent and extensive studies of progressively buried calcite inclusions confirm that calcite homogenization temperatures approach the maximum temperature of burial (Barker & Goldstein 1990) and these workers proposed that T_h be used as an independent geothermometer. Experimental studies of quartz inclusions indicate that quartz can also undergo either leakage (Bakker & Jansen 1990) or volume change, with smaller inclusions being less susceptible to re-equilibration (Sterner & Bodnar 1989).

The increase in T_h observed in this study in recovered

and deformed samples can be explained by a process of 'isochore jumping' whereby the homogenization temperature approaches the maximum temperature (Prezbindowski & Laresse 1987) during ductile deformation of quartz. In the present case, however, on account of the small size of the inclusions, it appears they did not stretch during ductile deformation, but rather they were destroyed by dislocation creep processes and subsequently reformed along subgrain boundaries and as isolated inclusions within subgrains. Drury & Urai (1990, p. 244) describe a process in which the interaction of a grain boundary with a fluid inclusion can result in the destruction of the fluid inclusion and the bleeding of the fluid onto the grain boundary. Subsequent necking down along the grain boundary is inferred to result in the formation of new inclusions. However, leakage along subgrain boundaries or change in pore volume during deformation or grain-boundary healing appears to be likely and maximum homogenization temperatures, therefore, are not likely to reflect the pressure conditions of trapping. In addition, the decrease in salinity of the inclusions toward the fault indicates that mixing with a low salinity fluid also took place during leakage and density re-equilibration. On the other hand, minimum T_h values may represent those inclusions that preserved the fluid density during trapping. If an independent estimate of temperature exists, the density of these inclusions can be used to constrain the fluid pressure conditions at the time of trapping (e.g. Roedder & Bodnar 1980), provided they have not been subsequently modified.

Two lines of evidence suggest that the inclusions displaying low T_h values have not been modified during post-tectonic processes: (1) the majority of inclusions measured are <5 μm in diameter; such inclusions can withstand excess internal pressures (i.e. $P_{internal} - P_{lithostatic}$) of >2 kb (Bodnar *et al.* 1989). Because the maximum lithostatic pressure was no greater than about 2.6 kb (see below) it is difficult to subject the inclusions to such large excess internal pressures during uplift; (2) the inclusions in plastically deformed samples do not lie on healed transgranular microfractures as would be expected for late stage inclusions produced during uplift.

In conclusion, maximum T_h values in deformed samples appear to reflect re-equilibration or leakage of inclusions to lower densities, and these T_h values are inferred to approach the maximum temperature conditions (approximately 300°C). Minimum T_h values, on the other hand, are interpreted to reflect the pressure conditions of trapping during crystal-plastic deformation of quartz.

Fluid pressure estimates

In the present study dynamic recrystallization of quartz is not extensive, but the temperature was sufficient such that dislocation creep processes were operative. Microstructures in polarized light indicate that dislocations were mobilized into subgrain arrays, giving rise to a polygonal texture (Fig. 3). On the basis of observations on natural rocks this suggests a temperature of about 300°C (Voll 1976). The similarity of microtextures in the variably deformed samples suggests that temperature variations between samples were not substantial. The inclusion homogenization temperature together with fluid salinities can be used to define fluid isochores (lines of constant density) in P–T space.

Table 1. Fluid pressures (kb) at 300°C*

Location	T_h (mode)	T_h (range)	T_m (mode)	P (range)	P (mode)
5	170	150–200	−16	2.7–1.8	2.3
6	200	150–300	−15	2.7–0.2	1.8
12	270	120–300	−12	3.4–0.2	0.5
17	250	160–300	−9	2.5–0.2	0.8
7	290	200–300	−11	1.8–0.2	0.2
16	170	140–260	−7	2.9–0.6	2.3

*Based on homogenization temperatures (T_h) and last melting temperatures (T_m) for NaCl–H_2O fluids using FLINCOR (Brown 1990).

Table 1 shows pressure estimates based on the maximum, modal and minimum homogenization temperatures (Fig. 4) and modal salinities (Fig. 5) for each locality, assuming a temperature of 300°C. Pressure estimates are based on the formulation of Brown & Lamb (1989) for NaCl–H_2O fluids, using the program FLINCOR (Brown 1990). In comparison to the range in homogenization temperature, ranges in salinity do not substantially affect these pressure estimates and only modal salinities are used. The calculated fluid pressures are plotted as a function of distance from the fault (Fig. 6c) using the data from Table 1.

A noteworthy feature of Fig. 6(c) is that the maximum pressures are close to, or above, lithostatic. All the samples shown are from bedding-parallel extensional veins. In order for extensional veins to form the following condition must be satisfied (Secor 1965, Fyfe *et al.* 1978):

$$P_{fluid} > S_3 + T_0,$$

where S_3 is the minimum principal stress and T_0 is the tensile strength of the rock. In a thrust setting, where S_3 is likely to be near vertical, and the veins formed parallel to bedding, P_{fluid} must exceed the lithostatic pressure; the maximum fluid pressures indicated on Fig. 6(c) are consistent with near lithostatic conditions. The wide range in minimum pressure estimates, which are substantially below hydrostatic conditions, suggests that the maximum homogenization temperatures (Fig. 6a) reflect re-equilibration of fluid inclusions to lower densities, rather than actual trapping conditions.

DISCUSSION

The depth to which surface-derived fluid can migrate freely in the continental crust depends to a large extent

on the depth to which the rock strength can withstand the difference between rock overburden pressure and fluid pressure, and thereby maintain an interconnected porosity. This depth is typically about 5 km (e.g. Wood & Walther 1986). Much deeper penetration, however, is likely along tectonically active faults where dilatancy would allow recharge of the fault zone under hydrostatic pressure (Costain *et al.* 1987, Nur & Walder 1990). Several lines of evidence (e.g. Crampin 1987, Scholz 1990) suggest that dilatancy is associated with fault rupture and a variety of dilatancy fluid-flow models involving tectonic pumping of fluids both upward (e.g. Scholz *et al.* 1973, Sibson *et al.* 1975) and downward (Costain *et al.* 1987, McCaig 1988) along fault zones to depths in excess of 10 km have been proposed.

Microstructural evidence indicates that shear and extension fractures occurred within the Rector Branch thrust (Figs. 2a & b) which, together with the hydration reactions, suggests that dilatancy played a role in allowing access of fluids to the fault zone. Dilatancy has the effect of increasing permeability and reducing fluid pressure conditions such that $P_{fluid} < P_{rock}$ (Brace 1972). On the other hand, the presence of bedding-parallel veins together with fluid-pressure estimates suggests hydrofracturing occurred, implying the condition $P_{fluid} \geqslant P_{rock}$ existed in the vicinity of and outside the fault zone. These combined observations suggest that fluid pressure fluctuated approximately between hydrostatic and lithostatic conditions. The decrease in salinity of fluids in vein quartz towards the fault suggests that the source of the low salinity fluid was from within the fault zone rather from the surrounding region. It is suggested that during periods of low fluid pressure surface-derived fluid may have infiltrated the fault zone at depth. An important test of this idea would be oxygen isotope analysis of the quartz veins which would be expected to display a decrease in $\delta^{18}O$ toward the fault.

Following recharge of the fault zone by surface-derived waters, reduction in permeability in the fault zone at depth would occur through a variety of time-dependent processes (e.g. fracture healing, pore collapse, solute precipitation, quartz plasticity, chemical reaction). This would seal the fault and result in the trapped fluid returning to lithostatic pressure (Nur & Walder 1990). Hydration reactions in the fault zone, by removing H_2O, could locally increase the salinity of trapped fluid (Crawford *et al.* 1979). The high salinity inclusions along healed microfractures in the fault zone rocks may represent samples of such fluid. Once lithostatic conditions are re-established hydraulic fracturing is likely to occur. In addition, low effective stress conditions on the fault will lead to rupture and expulsion of fault zone fluids rapidly upwards. Such a process would account for salinity and anomalous groundwater changes commonly associated with seismic events (e.g. Scholz 1990, p. 348). The migration of an undersaturated low salinity fluid downward against the thermal gradient would be an effective agent of dissolution and would explain the large bulk-rock volume losses previously reported from this fault zone (O'Hara 1988).

CONCLUSIONS

(1) The distribution of fluid inclusions along subgrain boundaries together with the wider range and higher T_h in deformed and recovered samples suggest that fluid densities have re-equilibrated to lower densities either during dislocation creep processes in quartz or during uplift. Minimum homogenization temperatures in vein quartz, however, indicate near-lithostatic conditions (2.6 kb at 300°C) and suggest that quartz veins represent hydrofracturing events.

(2) Decreasing salinity toward the fault is interpreted as due to infiltration of surface derived waters into the brittle–plastic transition (approximately 10 km) during periods of dilatancy. The higher salinity of fluids trapped along healed microfractures in the fault zone as compared to in the veins, may be the result of enhanced fluid–rock reaction in the fault zone.

(3) The salinity and fluid pressure variations observed are consistent with a dilatancy–hydrofracture model involving tectonic pumping of high-level fluid along the thrust zone. Low salinity, silica-undersaturated fluid flowing up the temperature and pressure gradients would be an effective agent of dissolution and would explain previously documented large bulk-rock volume losses from the Rector Branch thrust.

Acknowledgements—We thank two journal reviewers for helpful comments and Peter Hudleston for editorial handling. A grant to A. Haak from the southeast section of the Geological Society of America is appreciated.

REFERENCES

Bakker, R. J. & Jansen, B. H. 1990. Preferential water leakage from fluid inclusions by means of mobile dislocations. *Nature* **345**, 58–60.

Barker, C. E. & Goldstein, R. H. 1990. Fluid-inclusion technique for determining maximum temperature in calcite and its comparison to the vitrinite reflectance geothermometer. *Geology* **18**, 1003–1006.

Bodnar, R. J., Binns, P. R. & Hall, D. L. 1989. Synthetic fluid inclusions—VI. Quantitative evaluation of the decrepitation behavior of fluid inclusions in quartz at one atmosphere confining pressure. *J. metamorph. Geol.* **7**, 229–242.

Brace, W. F. 1972. Pore pressure in geophysics. In: *Flow and Fracture of Rocks* (edited by Spilhaus, A. F.). *Am. Geophys. Un. Geophys. Monogr.* **16**, 265–273.

Brown, P. E. 1990. FLINCOR: a microcomputer program for the reduction and investigation of fluid inclusion data. *Am. Miner.* **74**, 1390–1393.

Brown, P. E. & Lamb, W. M. 1989. P–V–T properties of fluids in the system H_2O –CO_2–NaCl: new graphical presentations and implications for fluid inclusion studies. *Geochim. cosmochim. Acta* **53**, 1209–1221.

Costain, J. K., Bollinger, G. A. & Speer, J. A. 1987. Hydroseismicity—a hypothesis for the role of water in the generation of intraplate seismicity. *Geology* **15**, 618–621.

Crampin, S. 1987. Geological and industrial implications of extensive-dilatancy anisotropy. *Nature* **328**, 491–496.

Crawford, M. L., Filer, J. & Wood, C. 1979. Saline fluid inclusions associated with retrograde metamorphism. *Bull. Minéral.* **102**, 562–568.

Drury, M. R. & Urai, J. L. 1990. Deformation-related recrystallization processes. *Tectonophysics* **172**, 235–253.

Etheridge, M. A., Wall, V. J. & Vernon, R. H. 1983. The role of the fluid phase during regional metamorphism and deformation. *J. metamorph. Geol.* **1**, 205–226.

Ferry, J. M. & Dipple, G. M. 1991. Fluid flow, mineral reactions, and metasomatism. *Geology* **19**, 211–214.

Fischer, G. J. & Paterson, M. S. 1989. Dilatancy during deformation of rocks at high temperatures and pressures. *J. geophys. Res.* **94**, 17,607–17,617.

Fournier, R. O., Rosenbauer, R. J. & Bischoff, L. 1982. The solubility of quartz in aqueous sodium chloride solutions at 350°C and 180 to 500 bars. *Geochim. cosmochim. Acta* **46**, 1975–1978.

Frape, S. K. & Fritz, P. 1986. Geochemical trends for groundwaters from the Canadian shield. In: *Saline Water and Gases in Crystalline Rocks* (edited by Fritz, P. & Frape, S. K.). *Spec. Pap. geol. Ass. Can.* **33**, 19–38.

Fyfe, W. S., Price, N. J. & Thompson, A. B. 1978. *Fluids in the Earth's Crust*. Elsevier, Amsterdam.

Glazner, A. F. & Bartley, J. M. 1991. Volume loss, fluid flow and state of strain in extensional mylonites from the central Mojave desert, California. *J. Struct. Geol.* **13**, 587–594.

Gratier, J. P. & Jenatton, L. 1984. Deformation by solution-deposition, and re-equilibration of fluid inclusions in crystals depending on temperature, internal pressure and stress. *J. Struct. Geol.* **6**, 189–200.

Haak, A. J. 1990. Fluid/rock interaction on the Rector Branch thrust, North Carolina, western Blue Ridge: A fluid inclusion study. Unpublished M.S. thesis, University of Kentucky, Lexington, Kentucky.

Hanor, S. J. 1976. The sedimentary genesis of hydrothermal fluids. In: *Geochemistry of Hydrothermal Ore Deposits* (2nd edn) (edited by Barnes, H. L.). Wiley, New York, 137–172.

Kerrich, R. 1976. Some aspects of tectonic recrystallization and fluid inclusions in vein quartz. *Contr. Miner. Petrol.* **59**, 195–202.

Kerrich, R. 1989. Geodynamic setting and hydraulic regimes: shear zone hosted mesothermal gold deposits. In: *Short Course Notes—Mineralization and Shear Zones* (edited by Bursnall, J. T.). *Geol. Ass. Can.* **6**, 89–128.

Lespinasse, M. & Cathelineau, M. 1990. Fluid inclusions in a fault zone: a study of fluid inclusion planes in the St Sylvestre granite, northwest Massif Central, France. *Tectonophysics* **184**, 173–187.

Losh, S. 1989. Fluid–rock interaction in an evolving ductile shear zone and across the brittle–ductile transition, Central Pyrenees, France. *Am. J. Sci.* **289**, 600–648.

McCaig, A. M. 1988. Deep fluid circulation in fault zones. *Geology* **16**, 865–960.

Nur, A. M. & Walder, J. 1990. Time-dependent hydraulics of the earth's crust. In: *The Role of Fluids in the Earth's Crust; Studies in Geophysics*. National Research Council, National Academy Press, Washington, DC, 113–127.

O'Hara, K. D. 1988. Fluid flow and volume loss during mylonitization: An origin for phyllonite in an overthrust setting. *Tectonophysics* **156**, 21–34.

O'Hara, K. D. 1990. State of strain in mylonites from the western Blue Ridge province, southern appalachians: the role of volume loss. *J. Struct. Geol.* **12**, 419–430.

O'Hara, K. D. & Blackburn, W. H. 1989. Volume loss model for trace element enrichments in mylonites. *Geology* **17**, 524–527.

Oriel, S. S. 1950. Geology and mineral resources of the Hot Springs window, Madison County, North Carolina. *Dept Conservation and Development Bull.* **60**.

Parry, W. T. & Bruhn, R. L. 1990. Fluid pressure transients on seismogenic normal faults. *Tectonophysics* **179**, 335–344.

Pêcher, A. 1981. Experimental decrepitation and re-equilibration of fluid inclusions in synthetic quartz. *Tectonophysics* **78**, 567–583.

Poirier, J.-P. 1985. *Creep of Crystals*. Cambridge University Press, Cambridge.

Potter, R. W. II, Clynne, M. A. & Brown, D. L. 1978. Freezing point depressions of aqueous sodium chloride solutions. *Econ. Geol.* **73**, 284–285.

Prezbindowski, D. R. & Laresse, R. E. 1987. Experimental stretching of fluid inclusions in calcite—implications for diagenetic studies. *Geology* **15**, 333–336.

Ramsay, J. G. 1980. The crack-seal mechanism of rock deformation. *Nature* **284**, 135–139.

Roedder, E. 1984. *Fluid Inclusions* (edited by Ribbe, H. P.). *Rev. Miner.* **12**.

Roedder, E. & Bodnar, R. J. 1980. Geologic pressure determinations from fluid inclusion studies. *Annu. Rev. Earth & Planet. Sci.* **80**, 263–301.

Reynolds, S. J. & Lister, G. 1987. Structural aspects of fluid–rock interactions in detachment zones. *Geology* **15**, 362–366.

Selverstone, J., Morteani, G. & Staude, J.-M. 1991. Fluid channeling during ductile shearing: transformation of granodiorite into aluminous schist in the Tauern window, Eastern Alps. *J. metamorph. Geol.* **9**, 419–431.

Scholz, C. H., Sykes, L. R. & Aggarwal, Y. P. 1973. Earthquake prediction: a physical basis. *Science* **181**, 803–810.

Scholz, C. H. 1990. *The Mechanics of Earthquakes and Faulting*. Cambridge University Press, Cambridge.

Secor, D. 1965. The role of fluid pressure in jointing. *Am. J. Sci.* **263**, 633–646.

Sibson, R. H., Moore, J. M. & Rankin, A. H. 1975. Seismic pumping—a hydrothermal fluid pumping mechanism. *J. geol. Soc. Lond.* **131**, 653–659.

Simpson, C. 1986. Fabric development in a brittle-to-ductile shear zone. *Pure & Appl. Geophys.* **124**, 269–288.

Sinha, A. K., Hewitt, D. A. & Rimstidt, J. D. 1986. Fluid interaction and element mobility in the development of ultramylonites. *Geology* **14**, 883–886.

Smith, D. L. & Evans, B. 1984. Diffusional crack healing in quartz. *J. geophys. Res.* **89**, 4125–4135.

Stel, H. 1986. The effect of cyclic operation of brittle and ductile deformation on the metamorphic assemblage in cataclasites and mylonites. *Pure & Appl. Geophys.* **124**, 289–307.

Sterner, S. M. & Bodnar, J. R. 1989. Synthetic fluid inclusions—VII. Re-equilibration of fluid inclusions in quartz during laboratory-simulated metamorphic burial and uplift. *J. metamorph. Geol.* **7**, 243–260.

Valley, J. W. 1986. Stable isotope geochemistry of metamorphic rocks. In: *Stable Isotopes* (edited by Ribbe, P. H.). *Rev. Miner.* **16**, 445–489.

Voll, G. 1976. Recrystallization of quartz, biotite and feldspar from Ertfeld to the Leventia Nappe, Swiss Alps and its geological significance. *Schweiz. miner. petrogr. Mitt.* **56**, 641–647.

White, J. C. & White, S. H. 1981. On the structure of grain boundaries in tectonites. *Tectonophysics* **78**, 613–628.

Wilkins, R. W. T. & Barkas, J. P. 1978. Fluid inclusions, deformation and recrystallization in granite tectonites. *Contr. Miner. Petrol.* **65**, 293–299.

Wood, B. J. & Walther, J. V. 1986. Fluid flow during metamorphism and its implications for fluid–rock ratios. In: *Fluid–rock Interactions During Metamorphism. Advances in Physical Geochemistry, Vol.* 5 (edited by Walther, J. V. & Wood, B. J.). Springer, New York, 109–131.